

Citation for published version:

Eames, C, Clark, JM, Rousse, G, Tarascon, J & Islam, MS 2014, 'Lithium migration pathways and van der Waals effects in the LiFeSO_4OH battery material', *Chemistry of Materials*, vol. 26, no. 12, pp. 3672-3678.
<https://doi.org/10.1021/cm5008203>

DOI:

[10.1021/cm5008203](https://doi.org/10.1021/cm5008203)

Publication date:

2014

Document Version

Peer reviewed version

[Link to publication](#)

University of Bath

Alternative formats

If you require this document in an alternative format, please contact:
openaccess@bath.ac.uk

General rights

Copyright and moral rights for the publications made accessible in the public portal are retained by the authors and/or other copyright owners and it is a condition of accessing publications that users recognise and abide by the legal requirements associated with these rights.

Take down policy

If you believe that this document breaches copyright please contact us providing details, and we will remove access to the work immediately and investigate your claim.

Lithium Migration Pathways and van der Waals Effects in the LiFeSO₄OH Battery Material

John M. Clark^a, Christopher Eames^a, Gwenaëlle Rousse^b, Jean-Marie Tarascon^c,
and M. Saiful Islam^{a*}

^a Department of Chemistry, University of Bath, Bath, BA2 7AY, United Kingdom

^b Institut de Minéralogie, de Physique des Matériaux, et de Cosmochimie (IMPMC), Sorbonne Universités - UPMC Univ Paris 06, UMR CNRS 7590, Muséum National d'Histoire Naturelle, IRD UMR 206, 4 Place Jussieu, F-75005 Paris, France

^c Réseau sur le Stockage Electrochimique de l'Energie (RS2E), FR CNRS 3459, Collège de France, 11 place Marcelin Berthelot, 75231 Paris Cedex 05, France

KEYWORDS (Word Style "BG_Keywords"). If you are submitting your paper to a journal that requires keywords, provide significant keywords to aid the reader in literature retrieval.

ABSTRACT: Layered LiFeSO₄OH has recently attracted interest as a sustainable cathode material for rechargeable lithium batteries that offers favorable synthesis and processing routes. Here, the defect chemistry, lithium-ion transport pathways and cell voltages of layered LiFeSO₄OH are investigated by atomistic modelling and density functional theory (DFT) methods and compared with the favorite polymorph. The results indicate that the layered phase exhibits two-dimensional (2D) lithium-ion diffusion with low activation energies of ~0.2 eV for long-range transport within the *bc*-plane, which is important for good rate capability. The favorite phase also shows 2D lithium-ion diffusion but with higher activation energies of ~0.7 eV. Using DFT+U techniques the experimental voltage and structural parameters are accurately reproduced for the favorite polymorph. For the layered structure, similar accuracy in both cell voltage and structure can only be obtained if a van der Waals functional is included in the DFT methodology to account for the interlayer binding.

1. INTRODUCTION

Alternative positive electrode materials to replace the LiCoO₂ system that is typically used within lithium ion batteries have attracted considerable attention.¹⁻⁴ The Co-based materials pose issues associated with cost and environmental hazard, particularly for large-scale storage applications (such as hybrid or electric vehicles and back-up power systems). Hence, the field of energy storage research has been particularly active in attempting to find new cathode materials for next-generation lithium ion batteries that may provide a solution to these problems.

To date, most interest has focused on the olivine-structured orthophosphate LiFePO₄,^{1,5} which is already in commercial use having exhibited favourable electrochemical properties. Despite this success, attention continues to be given to finding further examples of polyanionic-based compounds containing readily abundant Fe to act

as cathode materials in lithium batteries. In recent studies there have been changes in the polyanion and consequently the following materials have been proposed as alternative cathodes: Li₂FeSiO₄^{6,7} (160 mAh/g, 2.8 V vs Li/Li⁺); LiFeBO₃⁸ (200 mAh/g, 2.9 V vs Li/Li⁺); LiFeSO₄F^{9,10,11} which show polymorphism with both favorite and triplite showing redox capacities of 140 mAh/g at potentials of 3.6V and 3.9 V vs. Li/Li⁺ respectively; Li₂FePO₄F¹² (110 mAh/g, 3.4 V vs Li/Li⁺) and Li₂FeP₂O₇¹³ (110 mAh/g, 3.5 V vs Li/Li⁺).

Recently, it has been proposed that the newly synthesised layered iron hydroxysulphate¹⁴ (*P*₂/c), with composition LiFeSO₄OH and related compounds may provide a new avenue for positive electrode research. Direct synthesis of LiFeSO₄OH was provided by Tarascon et al.¹⁴ and results in the formation of a layered polymorph of the material. Electrochemical testing of the layered phase showed it to have a voltage of 3.6 V vs Li/Li⁺ for the

Fe²⁺/Fe³⁺ redox couple with a similar discharge capacity in the range 100–110 mAh/g observed upon cycling. As with LiFePO₄, the hydroxysulphate material is comprised of abundant and sustainable components. Although layered LiFeSO₄OH has a lower capacity than LiFePO₄ it does offer other advantages, which include a slightly higher potential, a lower synthesis temperature, and a favourable processing route as neither nanomaterials nor carbon coating are needed to utilize most of its capacity. Hence, these factors make LiFeSO₄OH a potential candidate for applications for which cost and abundance are essential.

In addition to the layered phase, tavorite-structured FeSO₄OH has been investigated by Reddy et al.¹⁵ Recent work by Tarascon et al.¹⁶ proposed this tavorite material to crystallise in the C2/c space group, into which Li could be inserted at a potential of 3.2 V vs Li/Li⁺ with a stable discharge capacity of ~110 mAh/g. The resulting lithiated composition of Li_xFeSO₄OH (*P*-1, where *x* < 1) for this tavorite is therefore prepared by electrochemical insertion of Li into FeSO₄OH and not by direct synthesis. Recent thermochemistry and calorimetric measurements¹⁷ find that layered LiFeSO₄OH is thermodynamically more stable than the tavorite polymorph.

The present study uses well-established atomistic simulation and density functional theory (DFT) techniques to investigate key solid-state issues for both layered and tavorite LiFeSO₄OH polymorphs. Atomistic simulation is well suited to treating the extensive lattice relaxation (up to several hundred ions) around charged defects and migrating ions in polar inorganic solids. DFT techniques have been applied successfully to analogous studies of other electrode materials for lithium batteries.^{18–22} The present work extends our recent computational studies of other polyanion-type cathodes such as LiFePO₄, Li₂MSiO₄ (*M* = Mn, Fe), Li₂FeSO₄F and Li₂FeP₂O₇.^{22–30}

2. SIMULATION METHODS

The atomistic and DFT techniques are described in detail elsewhere^{31,32}, and therefore only a general outline will be provided here. For the atomistic simulations, the interactions between ions in the hydroxysulphates polymorphs consist of a long-range Coulombic term and a short-range component representing electron-electron repulsion and van der Waals interactions. The short-range interactions were modeled using the two-body Buckingham potential³¹ and an additional three-body term was used for the SO₄^{2−} units as previously used for sulphates^{33–36}, silicates^{26–27} and phosphates^{23–25}. The shell model³⁷ was used to account for polarization effects induced by charged defects. The Li–O and O–O interatomic potentials were taken directly from the recent study of the related tavorite LiFeSO₄F whilst the Fe–O interaction was obtained by refining parameters from the same study³⁰. For the sulphate (SO₄) component, the interatomic potential model successfully formulated to simulate M₂SO₄ (*M* = Na, K, Rb and Cs) and XSO₄ (*X* = Sr, Ca, Ba)^{33–36} was used. For the hydroxyl (OH) group, the O–H interaction was modelled using an attractive Morse potential. This approach has recently been applied successfully to

protonic defects and water incorporation in fuel cell materials.^{38–40} Table S1 (supplementary information) lists the interatomic potential parameters used in this study. As argued previously, the validity of these interatomic potential methods are assessed primarily by their ability to reproduce observed crystal properties. Indeed, they are found to work well, even for compounds where there is undoubtedly a degree of covalency, such as phosphates, and silicates.^{23–28, 30}

The lattice relaxation about defects, (such as Li vacancies) and migrating ions was calculated by an implementation of the Mott-Littleton scheme incorporated in the GULP code.⁴² This method partitions the crystal lattice into two separate regions, where ions in the inner region immediately surrounding the defect (~1000 ions) are relaxed explicitly. It is worth noting that explicit relaxation of such a large number of lattice ions around defect species is not easily treated by electronic structure methods. For Li⁺ migration calculations, energy profiles for conduction paths can be derived by calculating the energy of the migrating ion between adjacent Li sites.

DFT calculations were carried out using the plane wave code VASP⁴³. The basis set was converged against the stress, which is more sensitive to an under-converged basis set than the forces. A cutoff energy of 850 eV with a *k*-point mesh density of at least 0.04 Å^{−1} was needed to adequately converge the stress (3 × 6 × 4 grid). PAW potentials^{44,45} and the PBE functional⁴⁶ were used. Our calculations employed full spin polarisation and an antiferromagnetic ordering of the moments on the Fe atoms was found to be lower in energy than a ferromagnetic ordering. Antiferromagnetism is common in iron sulphate-based cathode materials and has been observed in the related Li₂Fe(SO₄)₂, LiFeSO₄F and NaFeSO₄F compounds.^{11,47–49} DFT + *U* was used to correct the interactions inside for Fe *d*-orbitals with an effective Hubbard *U*_{eff} = *U* − *J* = 4 eV (*J* = 1 eV); this value is consistent with previous work on other Fe-based cathodes.^{19,21,50–51} We should emphasise that the focus of our DFT calculations is to enhance understanding of the trends in voltage differences which are not affected by the precise magnitude of the Hubbard *U* term.

Previous DFT studies on a range of oxide electrode materials^{18,22,32,52,53} have shown such methods to be well suited to probing lithium insertion/extraction properties and simulating precise trends in cell voltages. For both layered and tavorite polymorphs we have calculated the voltage for the Fe²⁺/Fe³⁺ redox couple using:

$$V = \frac{\epsilon\{\text{LiFeSO}_4\text{OH}\} - \epsilon\{\text{Li}_x\text{FeSO}_4\text{OH}\} - \{1-x\}\mu\{\text{Li}\}}{1-x} \quad (1)$$

where $\epsilon\{Y\}$ is the total energy of composition *Y* and *x* is the number of lithium atoms per formula unit removed, which in practice was one lithium atom per formula unit to produce the end member FeSO₄OH. Metallic lithium was used to calculate the chemical potential of a single

lithium atom $\mu\{\text{Li}\}$ which is standard practice for cell voltage calculations. To derive the cell voltage we have optimised the LiFeSO_4OH and FeSO_4OH structures and used their minimised energies in equation 1.

To investigate structural integrity on delithiation we have performed finite temperature annealing of the structure using *ab-initio* molecular dynamics (AIMD) in VASP with an NPT ensemble. The temperature was fixed at 50°C for all simulations using a Langevin thermostat and the equations of motion were controlled using the Verlet algorithm in VASP. A 0.5 fs timestep was employed to accurately capture the rapid motion of the light atomic species (H, Li) and each simulation was run for a total of 15 ps. A 264-atom supercell comprising $3 \times 3 \times 3$ unit cells was used and k-point sampling was only necessary at the gamma point for such a large system. To reduce the computational expense we used a cutoff energy of 500 eV and the FFT grids at a medium setting, which is standard practice in AIMD.

3. RESULTS AND DISCUSSION

3.1 STRUCTURES AND INTRINSIC ATOMIC DEFECTS

The starting point of the study was to reproduce the experimentally observed crystal structures. The layered- LiFeSO_4OH polymorph crystallizes in the monoclinic ($P2_1/c$) space group (Figure 1a), with edge-sharing FeO_6 octahedra that form a continuous zigzag chain that runs parallel to the b -axis direction. These chains are connected through shared oxygen vertices to form a layered structure. On each side of the layer of FeO_6 octahedra SO_4 tetrahedra are linked via oxygen vertices, hydroxyl groups form on the remaining oxygen vertices of the FeO_6 octahedra that are not shared with either SO_4 tetrahedra or other FeO_6 octahedra. Two of the oxygen vertices of the SO_4 tetrahedra are not shared with the FeO_6 octahedra and point into the open channel between the layers where the lithium resides, and as such the lithium atoms are tetrahedrally coordinated.

The delithiated tavorite- FeSO_4OH also crystallizes in the monoclinic space group. However with no experimental crystal structure reported for the tavorite- LiFeSO_4OH polymorph, the structure was set equivalent to that of the related the tavorite- LiFeSO_4F in the monoclinic ($P-1$) space group as suggested by Tarascon et. al¹⁴ who observed a structural change upon discharging the tavorite- FeSO_4OH ($C2/c$). Hence the structure of the tavorite- LiFeSO_4OH ($P-1$) polymorph (Figure 1b) is believed to include chains of alternately orientated corner-sharing $\text{FeO}_4(\text{OH})_2$ octahedra that run parallel to the c -axis direction and share hydroxyl groups located on opposite oxygen vertices. The remaining oxygen vertices of the FeO_6 octahedra are bonded to a sulphur atom forming Fe-O-S-O-Fe chains that cross-link the structure. Unlike the structure of the layered- LiFeSO_4OH polymorph, all of the oxygen vertices of the SO_4 tetrahedra are shared with the FeO_6 octahedra.

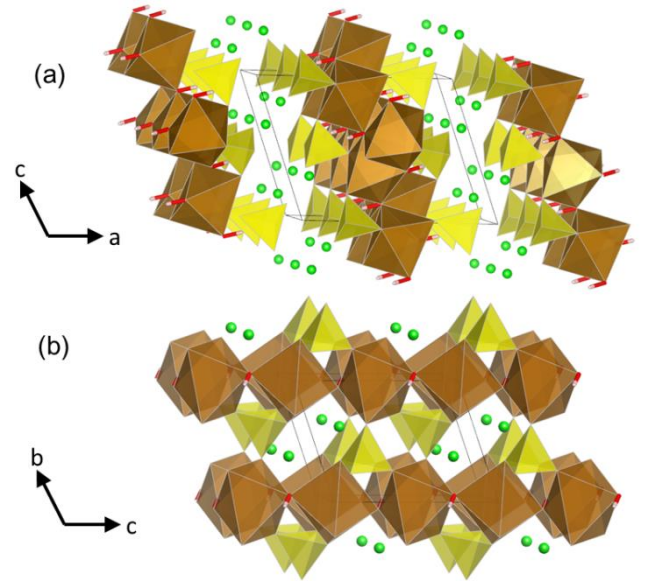
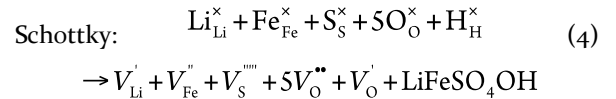
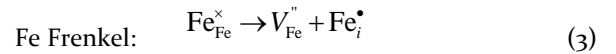
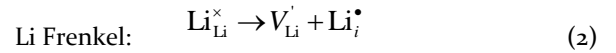


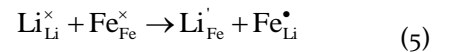
Figure 1. Crystal structures of (a) layered- and (b) tavorite- LiFeSO_4OH polymorphs showing FeO_6 octahedra (brown), SO_4 tetrahedra (yellow), OH bonds (red with cream tip) and lithium ions (green).

The calculated and experimental structures for the layered polymorph are given in Table S2, showing that the calculated unit cell parameters deviate from experiment by at most 0.09 Å, and in most cases by much less; the same is found for the Li-O, Fe-O, S-O and O-H bond lengths with mean deviations less than 0.06 Å. The accurate reproduction of the complex structure of the layered polymorph gives us confidence that the potential model can be utilized for a range of defect and migration calculations.

Atomic scale insights into the defect properties of cathode materials are crucial to gain a complete understanding of their behaviour. Isolated point defect (vacancy and interstitial) energies were calculated for both layered- and tavorite- LiFeSO_4OH , which were combined to derive the formation energies for Frenkel- and Schottky-type intrinsic defects. These defect reactions are represented by the following equations (using Kröger-Vink notation):



As in other polyanion cathodes, the Li/Fe “anti-site” pair defect is examined; this defect involves the exchange of a Li^+ ion (radius 0.74 Å) with an Fe^{2+} ion (radius 0.78 Å), according to:



Such Li/M anti-site or cation exchange effects have been observed in other polyanionic-type electrode materials including olivine LiMPO_4 ($M = \text{Mn, Fe, Co, Ni}$)^{23, 24, 54, 55} and $\text{Li}_2\text{FeP}_2\text{O}_7$ ³⁰. Therefore this type of defect is worth investigating here.

The resulting defect energies listed in Table 1 indicate two main features. First, all Frenkel and Schottky defects have unfavorable formation energies for both LiFeSO_4OH polymorphs. Second, the antisite energies are also relatively high, which suggests that there would be no significant concentration of Fe on Li sites at battery operating temperatures. This result contrasts with olivine LiFePO_4 ,²³ ($E_{\text{antisite}}=1.14$ eV) which exhibits anti-site behavior. Therefore these results suggest that conduction “blocking” effects involving Fe on Li sites are much less likely in the LiFeSO_4OH polymorphs.

Table 1. Energies of Intrinsic Atomic Defects in *layered-* and *tavorite-* LiFeSO_4OH

Disorder type	Equation	Energy (eV)	
		Layered	Tavorite
Li Frenkel	(2)	3.55	2.63
Fe Frenkel	(3)	6.38	7.97
Schottky	(4)	20.62	19.46
Li/Fe antisite	(5)	2.32	2.99

3.2 LITHIUM-ION DIFFUSION

Li ion mobility and diffusion pathways in LiFeSO_4OH are of vital importance when considering its rates of charge/discharge. However obtaining such insight for complex polyhedral structures from experiment is far from straightforward. Atomistic modeling methods allow us to examine the energetics and possible pathways for Li^+ conduction.

Figure 2 shows the different Li diffusion pathways considered within the layered- and tavorite- LiFeSO_4OH phases. We note that other pathways were considered but were found to be excessively high in energy (> 5 eV). Energy profiles for Li migration along each of these pathways can be mapped out. In this way the position of highest potential energy (i.e., the ‘saddle-point’ configuration) can be identified from which the migration energy is derived. The resulting lowest migration energies for Li diffusion along each of the five pathways are reported in Table 2.

The results reveal that the L1 and L2 pathways will allow the lowest energy Li diffusion within the layered-phase with energy barriers of 0.19 eV and 0.15 eV respectively. Such relatively low barriers suggest that the layered- LiFeSO_4OH will show high Li mobility, which is important for good electrochemical behaviour. The L1 and L2 pathways also involve the shortest Li-Li separations (3.13 Å and 3.49 Å respectively). Analysis of saddle-point configurations indicate lattice relaxation of local O, Fe, H and S ions of about 0.24, 0.09, 0.10 and 0.15 Å respectively, with the greatest displacement for adjacent O^{2-} ions as expected.

A higher activation energy barrier of 0.73 eV is calculated for the L3 pathway, which has a longer Li-Li separation of 4.16 Å. The remaining pathways (L4 and L5) are found to have high and unfavourable activation energies (> 2.80 eV) probably due to the migration distance exceeding 5 Å. Migration of Li ions from a bc -plane on one side of the layer of FeO_6 and SO_4 polyhedra to Li ions in the bc -plane on the other side would encounter separations of ≥ 8.0 Å in addition to significant steric hindrance, and needless to say these pathways are highly unfavourable.

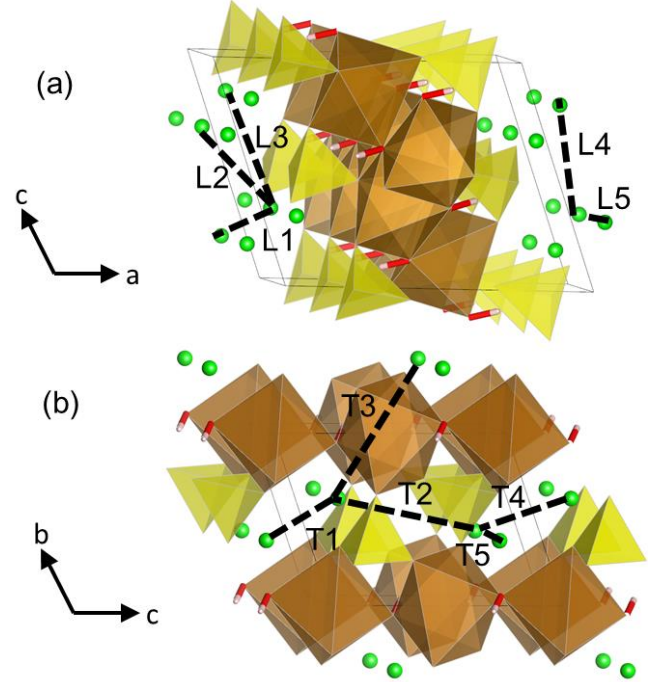


Figure 2. Li^+ migration pathways considered for (a) *layered-* and (b) *tavorite-* LiFeSO_4OH ; labelled L1-L5 and T1-T5 respectively in order of increasing Li-Li separation.

Table 2. Energies and Li-Li distances for Li Migration in (a) *layered-* and (b) *tavorite-* LiFeSO_4OH for paths shown in Figure 2.

(a) Layered- LiFeSO_4OH		
Path	Distance (Å)	E_{mig} (eV)
L1	3.13	0.19
L2	3.49	0.15
L3	4.16	0.73
L4	5.15	> 2.80
L5	5.51	> 2.80
(b) Tavorite- LiFeSO_4OH		
Path	Distance (Å)	E_{mig} (eV)
T1	3.35	0.38
T2	4.75	0.70
T3	4.80	> 2.50
T4	4.90	0.72
T5	5.18	> 2.50

In short, the combination of the highly favourable L1 and L2 migration pathways suggests that layered- LiFeSO_4OH will facilitate long-range diffusion along both the b -axis and c -axis directions, and as such the structure shows

two-dimensional (2D) Li migration within the bc -plane. The final simulated paths for long-range Li^+ diffusion are shown in Figure 3.

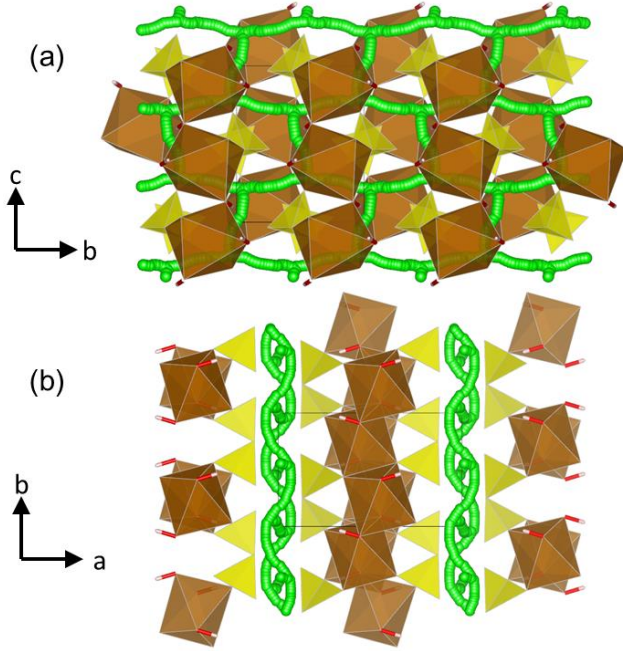


Figure 3. Calculated low energy pathways for long-range Li^+ migration along the b - and c -axis directions within layered- LiFeSO_4OH with activation energies of ≤ 0.19 eV; simulations indicate quasi-2D transport and non-linear trajectories (Li^+ pathways in green); (a) a -axis view; (b) c -axis view.

For the favorite-phase Table 2 reveals the T1, T2 and T4 pathways have the lowest energy barriers for Li diffusion of 0.38 eV, 0.70 eV and 0.72 eV respectively. These activation energy barriers for favorite- LiFeSO_4OH suggest much slower Li mobility as they are significantly higher than the corresponding values calculated for the layered-phase. The simulated paths for long-range Li^+ diffusion within favorite- LiFeSO_4OH are shown in Figure 4. The combination of the moderately favourable T1, T2 and T4 migration pathways suggests favorite- LiFeSO_4OH will facilitate long-range diffusion along both a -axis and c -axis directions, and as such the structure shows quasi-two-dimensional (2D) Li migration within the ac -plane.

Our simulations reveal curved paths between adjacent Li sites for both the layered- (Figure 3) and favorite- phases

(Figure 4), which produces “wave-like” trajectories for long-range migration. It is worth noting that analogous, curved Li^+ migration paths were first predicted from atomistic simulation studies of LiFePO_4 ²³ which were subsequently confirmed by neutron diffraction maximum entropy method (MEM) analysis⁵⁶.

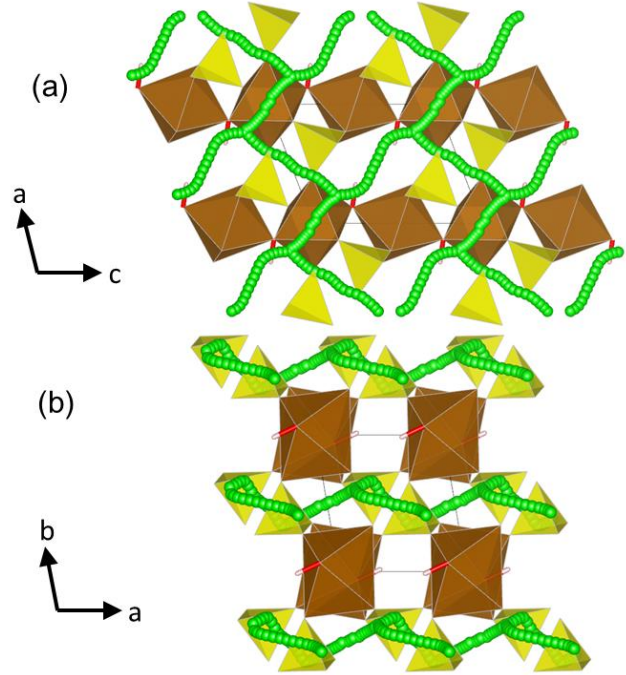


Figure 4. Calculated low energy pathways for long-range Li^+ migration along the a - and c -axis directions within favorite- LiFeSO_4OH with activation energies of ≤ 0.72 eV; simulations indicate quasi-2D transport and non-linear trajectories (Li^+ ion pathways in green); (a) b -axis view; (b) c -axis view.

3.3 BULK STRUCTURES AND CELL VOLTAGES

As with the potentials-based calculations we have also assessed various DFT-based methods in terms of the reproduction of the crystal structure and the cell voltage. Structural optimization of the as-prepared layered- LiFeSO_4OH ($P2_1/c$), layered- FeSO_4OH ($P2_1/c$) and favorite- FeSO_4OH ($C2/c$) was performed based on the crystal structures observed experimentally.¹⁴ There is no experimental crystal structure reported for the favorite-

Table 3. Structural parameters of layered LiFeSO_4OH and FeSO_4OH calculated with DFT and DFT+optPBE-vdW compared to experimental data¹⁴.

Layered LiFeSO_4OH					
	Expt	DFT+U	Δ	DFT+U+optPBE-vdW	Δ
a (Å)	9.5147(1)	9.7470	+0.2323	9.5655	+0.0508
b (Å)	5.5087(1)	5.5424	+0.0337	5.5099	+0.0012
c (Å)	7.3755(1)	7.4956	+0.1201	7.3950	+0.0195
β (°)	109.109(6)	110.020	+0.911	109.042	-0.067
Volume (Å ³)	365.28(1)	380.46	+15.18	368.42	+0.14
Layered FeSO_4OH					
	Expt*	DFT+U	Δ	DFT+U+optPBE-vdW	Δ
a (Å)	9.481(3)	9.7826	+0.3016	9.3698	-0.1112
b (Å)	5.296(2)	5.4023	+0.1063	5.3258	+0.0298
c (Å)	7.207(2)	7.4670	+0.2600	7.3756	+0.1686
β (°)	110.55(3)	111.661	+1.111	112.366	+1.816
Volume (Å ³)	338.9(2)	366.76	+27.86	340.37	+1.47

*Delithiated composition of $\text{Li}_{0.1}\text{FeSO}_4\text{OH}$

LiFeSO₄OH phase and therefore the structure was set equivalent to that of the related tavorite-LiFeSO₄F as suggested by Tarascon et. al.¹⁴ Cell voltage trends of LiFeSO₄F polymorphs have been examined previously by DFT+U calculations combined with crystallographic and electrostatic analyses²⁹. Our calculated energetics indicate that the layered polymorph of LiFeSO₄OH is thermodynamically more stable than tavorite, which agrees with recent calorimetry studies¹⁷.

In many layered materials such as graphite, boron nitride and V₂O₅, dispersion interactions between the layers are known to be significant.⁵⁷⁻⁵⁹ Since standard DFT methods do not include such van der Waals (vdW) interactions explicitly we have tested two types of vdW enhanced DFT schemes: semi-empirical vdW (Go6⁶⁰) and an explicit vdW exchange correlation functional (optPBE-vdW⁶¹). In general, we find that the latter vdW exchange correlation functional method better reproduces the structure and voltages of the layered phase; in the remainder of this work we report results obtained in this way. In Table S3 data generated using the semi-empirical vdW method are listed. We note that other recent studies have shown the significance of dispersion-corrected DFT in treating ion intercalation in graphite^{62,63} and organic cathode materials^{64,65} but there is limited work on inorganic polyanion-type cathodes.

The calculated structural parameters of layered LiFeSO₄OH and FeSO₄OH are presented in Table 3. It can be seen that using an explicit van der Waals functional (DFT+U+optPBE-vdW) provides a better agreement with the experimental structures than standard DFT+U. The improvement is mainly due to a more accurate interlayer spacing obtained by introducing dispersion interactions. The unit cell *a* parameter, which is almost parallel to the interlayer direction, can be used to assess the difference in the interlayer spacing between experiment and calculations. For LiFeSO₄OH the Δa difference with experiment is reduced from +2.4% with standard DFT to +0.5% with DFT+optPBE-vdW. For FeSO₄OH the Δa difference is reduced from +3.2% to -1.2%. We note here that the delithiated composition for the experimental structural data is Li_{0.1}FeSO₄OH; possible extraction of a further 0.1 Li per formula unit would decrease the interlayer spacing slightly, and closer to the calculated FeSO₄OH structure.

Using the total energies of these relaxed structures an average intercalation voltage has been derived for each phase according to equation 1 and these are listed in Table 4. For the layered phase the cell voltage computed when van der Waals effects are not included is severely overestimated by about 0.7 V, which is unusually large for DFT+U calculations. In contrast, the calculated voltage using optPBE-vdW is 3.87 V in much better agreement with the measured value of 3.6 V. To further understand this large contribution of van der Waals interactions to the computed voltage we must return to the structural parameters.

The agreement in interlayer spacing found for both layered LiFeSO₄OH and FeSO₄OH compositions on inclusion of vdW effects would suggest that these interactions

are important for interlayer binding. We have confirmed this by computing the binding energy versus the interlayer spacing. Such a binding potential is clearly present in the binding energy curve (Figure S1) with a minimum at the observed interlayer spacing. The stronger vdW interactions in FeSO₄OH reduce the energy difference between LiFeSO₄OH and FeSO₄OH, resulting in a lower voltage in accordance with equation 1. We recognize that numerous other interconnected factors contribute to the voltage of a material such as the energy of the transition metal redox couple, the Madelung energy and inductive effects, but van der Waals effects are also important for this layered hydroxysulphate.

Table 4. Comparison of calculated and experimental cell voltages (vs Li/Li⁺) for layered and tavorite hydroxysulphates.

Technique	Voltage (V)	
	Layered	Tavorite
Experiment	3.60	3.20
DFT+U	4.28	3.40
DFT+U+optPBE-vdW	3.87	3.40

As a comparison, we have also computed the voltage of the tavorite structure of LiFeSO₄OH using both standard DFT+U and DFT+U+optPBE-vdW. The calculated voltage of 3.40V vs 3.20V from experiment is not affected by the inclusion of vdW interactions; this result suggests that, as expected, dispersion interactions do not play a major role in the tavorite system. Nevertheless, the tavorite phase provides a useful ‘reference’ system to compare against layered LiFeSO₄OH and illustrates how significant the effect of vdW interactions is on the voltage of the layered phase.

Finally, we turn our attention to the question of possible proton mobility in these hydroxysulphate systems. Numerous mixed metal oxides and sulphates (e.g. CsHSO₄) are known to exhibit proton conductivity.^{66,67} It is therefore natural to question how tightly bound the proton is in the hydroxysulphates and whether any proton mobility is possible. The delithiated layered FeSO₄OH phase is the most likely candidate for proton mobility since the interlayer region is not occupied by Li ions. However, since full delithiation of this system is not found experimentally we modeled a composition of Li_{0.25}FeSO₄OH to test for proton mobility using *ab-initio* molecular dynamics with the vdW functional again included. The results indicate that the H atoms remain on-site and only exhibit the usual atomic vibrations. By contrast, if the same MD simulation is repeated with the vdW functional not included then proton transfer onto an SO₄ unit occurs within a short timescale (Figure S2), which has not been observed experimentally. This again indicates that vdW interactions in these calculations are essential in reproducing the observed properties of the ma-

terial and to the structural integrity of the delithiated phase.

4. CONCLUSIONS

This investigation of the layered-LiFeSO₄OH cathode material has used both atomistic modeling and density functional theory (DFT) techniques to examine the Li⁺ migration pathways and structural van der Waals effects. For comparison, we have also examined the favorite-structured phase.

Four main features emerge. First, the defect energy results suggest there would be no significant intrinsic concentration of Fe on Li sites in these hydroxysulphates at battery operating temperatures, in contrast to the LiFePO₄ material. Second, lithium diffusion in layered-LiFeSO₄OH follows curved pathways in the *bc*-plane with low migration energies (~0.2 eV), suggesting high Li mobility in a 2D network, which is important for good rate performance and capacity retention. Lithium diffusion within favorite-LiFeSO₄OH is found to have higher activation energies (~0.7 eV), suggesting much slower 2D Li mobility.

Third, DFT calculations show that there are significant interlayer van der Waals (vdW) interactions in the layered phase, which are not fully incorporated in conventional DFT. The reproduction of the experimental structure and voltage of layered LiFeSO₄OH is only achieved if these dispersion forces are included through an explicit van der Waals functional (DFT+U+optPBE-vdW). By contrast, the inclusion of van der Waals effects in the favorite phase does not alter the calculated structure or cell voltage, which are already in good agreement with experiment and indicate a key difference between the two LiFeSO₄OH structures. Finally, we note that *ab initio* MD simulations with the inclusion of vdW effects for the layered hydroxysulphate near to a state of full discharge (Li_{0.25}FeSO₄OH) show no evidence of proton mobility.

In general, this study indicates the importance of including van der Waals effects in DFT calculations on layered-structured materials for lithium-ion batteries, which have not been widely examined in inorganic polyanion-type cathodes.

Supporting Information. Interlayer binding energy curve for layered FeSO₄OH. Voltages computed with Go6 empirical vdW correction. Structural changes during AIMD annealing.

AUTHOR INFORMATION

Corresponding Author

*Prof. M. Saiful Islam, Email: m.s.islam@bath.ac.uk.

Author Contributions

All authors have given approval to the final version of the manuscript.

ACKNOWLEDGMENTS

This work was funded by EPSRC Supergen and Programme grants (EP/H019596/1, EP/K016288/1), and made use of the

high-performance computing service HECToR via the HPC Materials Chemistry Consortium (EP/F067496/1).

REFERENCES

- (1) Armand, M.; Tarascon, J. M. *Nature* **2008**, 451, 652.
- (2) Goodenough, J. B.; Kim, Y. *Chem. Mater.* **2010**, 22, 587.
- (3) Ellis, B. L.; Lee, K. T.; Nazar, L. F. *Chem. Mater.* **2010**, 22, 691.
- (4) Palacin, M. R. *Chem. Soc. Rev.* **2009**, 38, 2565.
- (5) Padhi, A. K.; Nanjundaswamy, K. S.; Goodenough, J. B. *J. Electrochem. Soc.* **1997**, 144, 1188.
- (6) Nyten, A.; Abouimrane, A.; Armand, M.; Gustafsson, T.; Thomas, J. O. *Electrochem. Commun.* **2005**, 7, 156.
- (7) Islam, M. S.; Dominko, R.; Masquelier, C.; Sirisopananaporn, C.; Armstrong, A. R.; Bruce, P. G. *J. Mater. Chem.* **2011**, 21, 9811.
- (8) Yamada, A.; Iwane, N.; Harada, Y.; Nishimura, S.; Koyama, Y.; Tanaka, I. *Adv. Mater.* **2010**, 22, 3583.
- (9) Recham, N.; Chotard, J. N.; Dupont, L.; Delacourt, C.; Walker, W.; Armand, M.; Tarascon, J. M. *Nature Mater.* **2010**, 9, 68.
- (10) Barpanda, P.; Ati, M.; Melot, B. C.; Rousse, G.; Chotard, J. N.; Doublet, M.-L.; Sougrati, M. T.; Corr, S. A.; Jumas, J.-C.; Tarascon, J.-M. *Nature Mater.* **2011**, 10, 772-779.
- (11) Rousse, G.; Tarascon, J.-M.; *Chem. Mater.* **2014**, 26, 394.
- (12) Ellis, B. L.; Makahnouk, W. R. M.; Makimura, Y.; Toghill, K.; Nazar, L. F. *Nat. Mater.* **2007**, 6, 749.
- (13) Nishimura, S.; Nakamura, M.; Natsui, R.; Yamada, A. *J. Am. Chem. Soc.* **2010**, 132, 13596.
- (14) Subban, C. V.; Ati, M.; Rousse, G.; Abakumov, A. M.; Van Tendeloo, G.; Janot, R.; Tarascon, J. M. *J. Am. Chem. Soc.* **2013**, 135, 3653.
- (15) Reddy, M. A.; Pralong, V.; Caignaert, V.; Varadaraju, U. V.; Raveau, B. *Electrochem. Commun.* **2009**, 11, 1807.
- (16) Ati, M.; Sougrati, M. T.; Rousse, G.; Recham, N.; Doublet, M. L.; Jumas, J. C.; Tarascon, J. M. *Chem. Mater.* **2012**, 24, 1472.
- (17) Radha, A. V.; Subban, C. V.; Sun, M. L.; Tarascon, J. M.; Navrotsky, A. *J. Mater. Chem.* **2014**, 2, 6887.
- (18) Zhou, F.; Cococcioni, M.; Marianetti, C. A.; Morgan, D.; Ceder, G. *Phys. Rev. B* **2004**, 70, 23.
- (19) Zhou, H.; Upreti, S.; Chernova, N. A.; Hautier, G.; Ceder, G.; Whittingham, M. S. *Chem. Mater.* **2011**, 23, 293.
- (20) Hautier, G.; Jain, A.; Chen, H. L.; Moore, C.; Ong, S. P.; Ceder, G. *J. Mater. Chem.* **2011**, 21, 17147.
- (21) Armstrong, A. R.; Lyness, C.; Panchmatia, P. M.; Islam, M. S.; Bruce, P. G. *Nat. Mater.* **2011**, 10, 223.
- (22) Eames, C.; Armstrong, A. R.; Bruce, P. G.; Islam, M. S. *Chem. Mater.* **2012**, 24, 2155.
- (23) Islam, M. S.; Driscoll, D. J.; Fisher, C. A. J.; Slater, P. R. *Chem. Mater.* **2005**, 17, 5085.
- (24) Fisher, C. A. J.; Prieto, V. M. H.; Islam, M. S. *Chem. Mater.* **2008**, 20, 5907.
- (25) Gardiner, G. R.; Islam, M. S. *Chem. Mater.* **2010**, 22, 1242.
- (26) Kuganathan, N.; Islam, M. S. *Chem. Mater.* **2009**, 21, 5196.
- (27) Armstrong, A. R.; Kuganathan, N.; Islam, M. S.; Bruce, P. G. *J. Am. Chem. Soc.* **2011**, 133, 13031.
- (28) Tripathi, R.; Gardiner, G. R.; Islam, M. S.; Nazar, L. F. *Chem. Mater.* **2011**, 23, 2278.
- (29) Yahia, M. B.; Lemoigno, F.; Rousse, G.; Boucher, F.; Tarascon, J.-M.; Doublet, M.-L. *Energy Environ. Sci.* **2012**, 5, 9584.
- (30) Clark, J. M.; Nishimura, S.; Yamada, A.; Islam, M. S. *Angew. Chem. Int. Ed.* **2012**, 51, 13149.
- (31) Catlow, C. R. A., *Computer Modelling in Inorganic Crystallography*. In Academic Press: San Diego: **1997**.
- (32) Islam, M. S.; Fisher, C. A. J.; *Chem. Soc. Rev.*, **2014**, 43, 185.
- (33) Allan, N. L.; Rohl, A. L.; Gay, D. H.; Catlow, C. R. A.; Davey, R. J.; Mackrodt, W. C., *Faraday Discuss.* **1993**, 95, 273.

- (34) Redfern, S. E.; Parker, S. C. *J. Chem. Soc., Faraday Trans.* **1998**, 94, 1947.
- (35) Sastre, G.; Gale, J. D. *Chem. Mater.* **2005**, 17, 730.
- (36) Gomez-Hortiguela, L.; Cora, F.; Catlow, C. R. A.; Perez-Pariente, J. J. *Am. Chem. Soc.* **2004**, 126, 12097.
- (37) Dick, B. G.; Overhauser, A. W. *Phys. Rev.* **1958**, 112, 90.
- (38) Panchmatia, P. M.; Orera, A.; Kendrick, E.; Hanna, J. V.; Smith, M. E.; Slater, P. R.; Islam, M. S. *J. Mater. Chem.* **2010**, 20, 2766.
- (39) Stokes, S. J.; Islam, M. S. *J. Mater. Chem.* **2010**, 20, 6258.
- (40) Panchmatia, P. M.; Orera, A.; Rees, G. J.; Smith, M. E.; Hanna, J. V.; Slater, P. R.; Islam, M. S. *Angew. Chem. Int. Ed.* **2011**, 50, 9328.
- (41) Henson, N. J.; Hay, P. J.; Redondo, A. *J. Phys. Chem. A* **2000**, 104, 2423.
- (42) Gale, J. D.; Rohl, A. L. *Mol. Simul.* **2003**, 29, 291.
- (43) Kresse, G.; Furthmüller, J. *Phys. Rev. B* **1996**, 54, 11169.
- (44) Blochl, P. E. *Phys. Rev. B* **1994**, 50, 17953.
- (45) Kresse, G.; Joubert, D. *Phys. Rev. B* **1999**, 59, 1758.
- (46) Perdew, J. P.; Burke, K.; Ernzerhof, M. *Phys. Rev. Lett.* **1996**, 77, 3865.
- (47) Reynaud, M.; Rousse, G.; Chotard, J.-N.; Carvajal, J. R.; Tarascon, J.-M.; *Inorg. Chem.* **2013**, 52, 10456.
- (48) Melot, B. C.; Rousse, G.; Chotard, J.-N.; Ati, M.; Carvajal, J. R.; Kemei, M. C.; Tarascon, J.-M.; *Chem. Mater.* **2011**, 23, 2922.
- (49) Melot, B. C. et al *Phys. Rev. B.*, **2012**, 85, 094415.
- (50) Zhou, F.; Cococcioni, M.; Kang, K.; Ceder, G. *Electrochem. Commun.* **2004**, 6, 1144.
- (51) Arroyo-de Dompablo, M. E.; Armand, M.; Tarascon, J. M.; Amador, U. *Electrochem. Commun.* **2006**, 8, 1292.
- (52) Ceder, G.; Aydinol, M. K.; Kohan, A. F. *Comp. Mater. Sci.* **1997**, 8, 161.
- (53) Arrouvel, C.; Parker, S. C.; Islam, M. S. *Chem. Mater.* **2009**, 21, 4778.
- (54) Maier, J.; Amin, R. *J. Electrochem. Soc.* **2008**, 155, A339.
- (55) Chen, J. J.; Vacchio, M. J.; Wang, S. J.; Chernova, N.; Zavalij, P. Y.; Whittingham, M. S. *Solid State Ionics* **2008**, 178, 1676.
- (56) Nishimura, S.; Kobayashi, G.; Ohoyama, K.; Kanno, R.; Yashima, M.; Yamada, A. *Nat. Mater.* **2008**, 7, 707.
- (57) Rydberg, H.; Dion, M.; Jacobson, N.; Schroder, E.; Hylgaard, P.; Simak, S. I.; Langreth, D. C.; Lundqvist, B. I.; *Phys. Rev. Lett.* **2003**, 91, 126402.
- (58) Bucko, T.; Hafner, J.; Lebegue, S.; Angyan, J. G.; *J. Phys. Chem. A* **2010**, 114, 11814.
- (59) Marom, N.; Bernstein, J.; Garel, J.; Tkatchenko, A.; Joselevich, E.; Kronik, L.; Hod, O.; *Phys. Rev. Lett.* **2010**, 105, 046801.
- (60) Grimme, S.; *J. Comp. Chem.* **2006**, 27, 1787.
- (61) Klimes, J.; Bowler, D. R.; Michaelides, A.; *Phys. Rev. B.* **2011**, 83, 195131.
- (62) Persson, K.; Hinuma, Y.; Meng, Y. S.; Van der Ven, A.; Ceder, G. *Phys. Rev. B.* **2010**, 82, 125416.
- (63) Wang, Z.; Selbach, S. M.; Grande, T. *RSC Advances* **2014**, 4, 4069.
- (64) Frayret, C.; Ekaterina, I.; Izgorodina, E.; MacFarlane, D. R.; Villesuzanne, A.; Barrès, A.-L.; Politano, O.; Rebeixd, D.; Poizota, P. *Phys. Chem. Chem. Phys.* **2012**, 14, 11398.
- (65) Ramos-Sanchez, G.; Callejas-Tovar A.; Scanlon, L. G.; Balbuena, P. B. *Phys. Chem. Chem. Phys.* **2014**, 16, 743–52.
- (66) Kreuer, K. D.; *Ann. Rev. Mat. Res.* **2003**, 33, 333.
- (67) Malavasi, L.; Fisher, C. A. J.; Islam, M. S.; *Chem. Soc. Rev.* **2010**, 39, 4370.

